Eur. Phys. J. C 13, 1–13 (2000)
Digital Object Identifier (DOI) 10.1007/s100520000260

THE EUROPEAN PHYSICAL JOURNAL C

Measurement of the production rate of charm quark pairs from gluons in hadronic Z^0 decays

The OPAL Collaboration

G. Abbiendi[2], K. Ackerstaff[8], G. Alexander[23], J. Allison[16], K.J. Anderson[9], S. Anderson[12], S. Arcelli[17], S. Asai[24], S.F. Ashby[1], D. Axen[29], G. Azuelos[18,a], A.H. Ball[8], E. Barberio[8], R.J. Barlow[16], J.R. Batley[5], S. Baumann[3], J. Bechtluft[14], T. Behnke[27], K.W. Bell[20], G. Bella[23], A. Bellerive[9], S. Bentvelsen[8], S. Bethke[14], S. Betts[15], O. Biebel[14], A. Biguzzi[5], I.J. Bloodworth[1], P. Bock[11], J. Böhme[14], O. Boeriu[10], D. Bonacorsi[2], M. Boutemeur[33], S. Braibant[8], P. Bright-Thomas[1], L. Brigliadori[2], R.M. Brown[20], H.J. Burckhart[8], P. Capiluppi[2], R.K. Carnegie[6], A.A. Carter[13], J.R. Carter[5], C.Y. Chang[17], D.G. Charlton[1,b], D. Chrisman[4], C. Ciocca[2], P.E.L. Clarke[15], E. Clay[15], I. Cohen[23], J.E. Conboy[15], O.C. Cooke[8], J. Couchman[15], C. Couyoumtzelis[13], R.L. Coxe[9], M. Cuffiani[2], S. Dado[22], G.M. Dallavalle[2], S. Dallison[16], R. Davis[30], S. De Jong[12], A. de Roeck[8], P. Dervan[15], K. Desch[27], B. Dienes[32,h], M.S. Dixit[7], M. Donkers[6], J. Dubbert[33], E. Duchovni[26], G. Duckeck[33], I.P. Duerdoth[16], P.G. Estabrooks[6], E. Etzion[23], F. Fabbri[2], A. Fanfani[2], M. Fanti[2], A.A. Faust[30], L. Feld[10], P. Ferrari[12], F. Fiedler[27], M. Fierro[2], I. Fleck[10], A. Frey[8], A. Fürtjes[8], D.I. Futyan[16], P. Gagnon[7], J.W. Gary[4], G. Gaycken[27], C. Geich-Gimbel[3], G. Giacomelli[2], P. Giacomelli[2], W.R. Gibson[13], D.M. Gingrich[30,a], D. Glenzinski[9], J. Goldberg[22], W. Gorn[4], C. Grandi[2], K. Graham[28], E. Gross[26], J. Grunhaus[23], M. Gruwé[27], C. Hajdu[31] G.G. Hanson[12], M. Hansroul[8], M. Hapke[13], K. Harder[27], A. Harel[22], C.K. Hargrove[7], M. Harin-Dirac[4], M. Hauschild[8], C.M. Hawkes[1], R. Hawkings[27], R.J. Hemingway[6], G. Herten[10], R.D. Heuer[27], M.D. Hildreth[8], J.C. Hill[5], P.R. Hobson[25], A. Hocker[9], K. Hoffman[8], R.J. Homer[1], A.K. Honma[28,a], D. Horváth[31,c], K.R. Hossain[30], R. Howard[29], P. Hüntemeyer[27], P. Igo-Kemenes[11], D.C. Imrie[25], K. Ishii[24], F.R. Jacob[20], A. Jawahery[17], H. Jeremie[18], M. Jimack[1], C.R. Jones[5], P. Jovanovic[1], T.R. Junk[6], N. Kanaya[24], J. Kanzaki[24], D. Karlen[6], V. Kartvelishvili[16], K. Kawagoe[24], T. Kawamoto[24], P.I. Kayal[30], R.K. Keeler[28], R.G. Kellogg[17], B.W. Kennedy[20], D.H. Kim[19], A. Klier[26], T. Kobayashi[24], M. Kobel[3,d], T.P. Kokott[3], M. Kolrep[10], S. Komamiya[24], R.V. Kowalewski[28], T. Kress[4], P. Krieger[6], J. von Krogh[11], T. Kuhl[3], P. Kyberd[13], G.D. Lafferty[16], H. Landsman[22], D. Lanske[14], J. Lauber[15], I. Lawson[28], J.G. Layter[4], D. Lellouch[26], J. Letts[12], L. Levinson[26], R. Liebisch[11], J. Lillich[10], B. List[8], C. Littlewood[5], A.W. Lloyd[1], S.L. Lloyd[13], F.K. Loebinger[16], G.D. Long[28], M.J. Losty[7], J. Lu[29], J. Ludwig[10], D. Liu[12], A. Macchiolo[18], A. Macpherson[30], W. Mader[3], M. Mannelli[8], S. Marcellini[2], T.E. Marchant[16], A.J. Martin[13], J.P. Martin[18], G. Martinez[17], T. Mashimo[24], P. Mättig[26], W.J. McDonald[30], J. McKenna[29], E.A. Mckigney[15], T.J. McMahon[1], R.A. McPherson[28], F. Meijers[8], P. Mendez-Lorenzo[33], F.S. Merritt[9], H. Mes[7], I. Meyer[5], A. Michelini[2], S. Mihara[24], G. Mikenberg[26], D.J. Miller[15], W. Mohr[10], A. Montanari[2], T. Mori[24], K. Nagai[8], I. Nakamura[24], H.A. Neal[12,g], R. Nisius[8], S.W. O'Neale[1], F.G. Oakham[7], F. Odorici[2], H.O. Ogren[12], A. Okpara[11], M.J. Oreglia[9], S. Orito[24], G. Pásztor[31], J.R. Pater[16], G.N. Patrick[20], J. Patt[10], R. Perez-Ochoa[8], S. Petzold[27], P. Pfeifenschneider[14], J.E. Pilcher[9], J. Pinfold[30], D.E. Plane[8], P. Poffenberger[28], B. Poli[2], J. Polok[8], M. Przybycień[8,e], A. Quadt[8], C. Rembser[8], H. Rick[8], S. Robertson[28], S.A. Robins[22], N. Rodning[30], J.M. Roney[28], S. Rosati[3], K. Roscoe[16], A.M. Rossi[2], Y. Rozen[22], K. Runge[10], O. Runolfsson[8], D.R. Rust[12], K. Sachs[10], T. Saeki[24], O. Sahr[33], W.M. Sang[25], E.K.G. Sarkisyan[23], C. Sbarra[29], A.D. Schaile[33], O. Schaile[33], P. Scharff-Hansen[8], J. Schieck[11], S. Schmitt[11], A. Schöning[8], M. Schröder[8], M. Schumacher[3], C. Schwick[8], W.G. Scott[20], R. Seuster[14], T.G. Shears[8], B.C. Shen[4], C.H. Shepherd-Themistocleous[5], P. Sherwood[15], G.P. Siroli[2], A. Skuja[17], A.M. Smith[8], G.A. Snow[17], R. Sobie[28], S. Söldner-Rembold[10,f], S. Spagnolo[20], M. Sproston[20], A. Stahl[3], K. Stephens[16], K. Stoll[10], D. Strom[19], R. Ströhmer[33], B. Surrow[8], S.D. Talbot[1], P. Taras[18], S. Tarem[22], R. Teuscher[9], M. Thiergen[10], J. Thomas[15], M.A. Thomson[8], E. Torrence[8], S. Towers[6], T. Trefzger[33], I. Trigger[18], Z. Trócsányi[32,h], E. Tsur[23], M.F. Turner-Watson[1], I. Ueda[24], R. Van Kooten[12], P. Vannerem[10], M. Verzocchi[8], H. Voss[3], F. Wäckerle[10], A. Wagner[27], D. Waller[6], C.P. Ward[5], D.R. Ward[5], P.M. Watkins[1], A.T. Watson[1], N.K. Watson[1], P.S. Wells[8], N. Wermes[3], D. Wetterling[11] J.S. White[6], G.W. Wilson[16], J.A. Wilson[1], T.R. Wyatt[16], S. Yamashita[24], V. Zacek[18], D. Zer-Zion[8]

[1] School of Physics and Astronomy, University of Birmingham, Birmingham B15 2TT, UK
[2] Dipartimento di Fisica dell' Università di Bologna and INFN, 40126 Bologna, Italy
[3] Physikalisches Institut, Universität Bonn, 53115 Bonn, Germany
[4] Department of Physics, University of California, Riverside CA 92521, USA
[5] Cavendish Laboratory, Cambridge CB3 0HE, UK
[6] Ottawa-Carleton Institute for Physics, Department of Physics, Carleton University, Ottawa, Ontario K1S 5B6, Canada
[7] Centre for Research in Particle Physics, Carleton University, Ottawa, Ontario K1S 5B6, Canada

[8] CERN, European Organisation for Particle Physics, 1211 Geneva 23, Switzerland
[9] Enrico Fermi Institute and Department of Physics, University of Chicago, Chicago IL 60637, USA
[10] Fakultät für Physik, Albert Ludwigs Universität, 79104 Freiburg, Germany
[11] Physikalisches Institut, Universität Heidelberg, 69120 Heidelberg, Germany
[12] Indiana University, Department of Physics, Swain Hall West 117, Bloomington IN 47405, USA
[13] Queen Mary and Westfield College, University of London, London E1 4NS, UK
[14] Technische Hochschule Aachen, III Physikalisches Institut, Sommerfeldstrasse 26-28, 52056 Aachen, Germany
[15] University College London, London WC1E 6BT, UK
[16] Department of Physics, Schuster Laboratory, The University, Manchester M13 9PL, UK
[17] Department of Physics, University of Maryland, College Park, MD 20742, USA
[18] Laboratoire de Physique Nucléaire, Université de Montréal, Montréal, Quebec H3C 3J7, Canada
[19] University of Oregon, Department of Physics, Eugene OR 97403, USA
[20] CLRC Rutherford Appleton Laboratory, Chilton, Didcot, Oxfordshire OX11 0QX, UK
[22] Department of Physics, Technion-Israel Institute of Technology, Haifa 32000, Israel
[23] Department of Physics and Astronomy, Tel Aviv University, Tel Aviv 69978, Israel
[24] International Centre for Elementary Particle Physics and Department of Physics, University of Tokyo, Tokyo 113-0033, and Kobe University, Kobe 657-8501, Japan
[25] Institute of Physical and Environmental Sciences, Brunel University, Uxbridge, Middlesex UB8 3PH, UK
[26] Particle Physics Department, Weizmann Institute of Science, Rehovot 76100, Israel
[27] Universität Hamburg/DESY, II Institut für Experimental Physik, Notkestrasse 85, 22607 Hamburg, Germany
[28] University of Victoria, Department of Physics, P O Box 3055, Victoria BC V8W 3P6, Canada
[29] University of British Columbia, Department of Physics, Vancouver BC V6T 1Z1, Canada
[30] University of Alberta, Department of Physics, Edmonton AB T6G 2J1, Canada
[31] Research Institute for Particle and Nuclear Physics, H-1525 Budapest, P O Box 49, Hungary
[32] Institute of Nuclear Research, H-4001 Debrecen, P O Box 51, Hungary
[33] Ludwigs-Maximilians-Universität München, Sektion Physik, Am Coulombwall 1, 85748 Garching, Germany

Received: 30 June 1999 / Published online: 3 February 2000 –

Abstract. The rate of secondary charm-quark-pair production has been measured in 4.4 million hadronic Z^0 decays collected by OPAL. By selecting events with three jets and tagging charmed hadrons in the gluon jet candidate using leptons and $D^{\star\pm}$ mesons, the average number of secondary charm-quark pairs per hadronic event is found to be $(3.20\pm0.21\pm0.38)\times10^{-2}$.

1 Introduction

The production of secondary heavy quarks from a virtual gluon is commonly referred to as gluon splitting. This process is considerably suppressed because both the gluon and the quark jet from which it originates must be sufficiently virtual to produce the heavy-quark pair. Nonetheless, these events make a significant contribution to heavy quark pair production in e+e- annihilation: $e^+e^-\to q\overline{q}g$, $g\to Q\overline{Q}$, where Q is a bottom or charm quark. These events will be referred to here as $g\to c\overline{c}$ or $g\to b\overline{b}$ events. This paper describes a measurement of the rate of $g\to c\overline{c}$ at LEP at center-of-mass energies in the region of the Z^0 peak.

The probability of producing a heavy-quark pair from a gluon, per hadronic Z^0 decay, is defined as

$$g_{Q\overline{Q}} = \frac{N(Z^0 \to q\overline{q}g, g \to Q\overline{Q})}{N(Z^0 \to \text{hadrons})}. \quad (1)$$

This probability has been calculated in the framework of perturbative QCD to leading order in α_s, with the resummation of large leading and next-to-leading logarithmic terms to all orders [1–4]. The probabilities for the secondary production of a charm-quark or bottom-quark pair are predicted to be in the range $(1.35\text{–}2.01)\times10^{-2}$ for $g_{c\overline{c}}$, and $(1.75\text{–}2.90)\times10^{-3}$ for $g_{b\overline{b}}$. Precise measurements of these quantities allow an important comparison with QCD calculations, and also reduce the uncertainty in the experimental determination of electroweak variables, such as R_c, the fraction of $Z^0\to c\overline{c}$ events in hadronic Z^0 decays.

The first measurement of $g_{c\overline{c}}$ was made by OPAL [5], where the contribution from the process $g\to c\overline{c}$ to the inclusive $D^{\star\pm}$ meson momentum spectrum was obtained by subtracting the contribution from $Z^0\to c\overline{c}$ and $Z^0\to b\overline{b}$ events where the $D^{\star\pm}$ was produced from a primary quark. This was followed by a second OPAL analysis [6], in which gluon jets were selected, and charmed hadrons in these jets were identified by a lepton tag. Combining the two measurements gave $g_{c\overline{c}}= (2.38\pm0.48)\times10^{-2}$ [6], a value which

[a] and at TRIUMF, Vancouver, Canada V6T 2A3
[b] and Royal Society University Research Fellow
[c] and Institute of Nuclear Research, Debrecen, Hungary
[d] on leave of absence from the University of Freiburg
[e] and University of Mining and Metallurgy, Cracow
[f] and Heisenberg Fellow
[g] now at Yale University, Dept of Physics, New Haven, USA
[h] and Department of Experimental Physics, Lajos Kossuth University, Debrecen, Hungary

is compatible with the upper range of the theoretical predictions.

The ALEPH and DELPHI collaborations have recently measured the rate of secondary production of b-quark pairs to be $g_{b\bar{b}}=(2.77\pm0.42\pm0.57)\times10^{-3}$ [7] and $g_{b\bar{b}}=(2.1\pm1.1\pm0.9)\times10^{-3}$ [8] respectively. Both measurements are consistent with theoretical predictions.

The existing OPAL measurements [5,6] only analysed part of the total Z^0 data sample. In this analysis the full sample was used. The precision of this measurement was further improved with a more refined data calibration, optimisation of the analysis algorithms, and a more reliable Monte Carlo simulation of the OPAL detector. To establish a signature for secondary charm-quark-pair production, events containing three jets were selected, and the gluon jet identified. The charm content of the gluon jet candidate was analysed by identifying electrons, muons, and $D^{\star\pm}$ mesons, to give three independent measurements of $g\to c\bar{c}$. The analysis is presented as follows: Section 2 describes the hadronic sample and event simulation; Section 3 discusses the selection of events likely to contain a hard gluon and the methods used to select the gluon jet; this is followed by a description of the lepton and $D^{\star\pm}$ channels separately in Sects. 4 and 5; the systematic uncertainties for all the tagging schemes are listed in Sect. 6; the paper concludes with a summary in Sect. 7.

2 Hadronic event selection and simulation

We used data collected at LEP by the OPAL detector [9] between 1990 and 1995 in the vicinity of the Z^0 peak. Hadronic Z^0 decays were selected using the number of charged tracks and the visible energy in each event as in Reference [10]. This selection yielded 4.41 million events. The primary vertex of the event was reconstructed using the charged tracks in the event and the knowledge of the position and spread of the e^+e^- collision point.

Monte Carlo events were used to determine the selection efficiency and background levels. The selection efficiency was measured in dedicated samples of events containing the $g\to c\bar{c}$ process. For the lepton analysis, at least one of the charmed hadrons was required to decay semileptonically. The $D^{\star\pm}$ analysis used events where at least one of the secondary charm quarks hadronised to a $D^{\star\pm}$ which decayed via $D^{\star+}\to D^0\pi^+$, followed by $D^0\to K^-\pi^{+1}$. For background studies, 9 million 5-flavour hadronic Z^0 decays plus an additional 3.5 million $Z^0\to b\bar{b}$ events and 2.5 million $Z^0\to c\bar{c}$ events were generated. All these samples were produced with the JETSET 7.4 Monte Carlo program [11]. The heavy quark fragmentation was parametrized by the fragmentation function of Peterson et al. [12], and the measured values of the partial widths of Z^0 into $q\bar{q}$ were used [13]. The production rates of different charmed hadrons at $\sqrt{s}=10\,\mathrm{GeV}$ and $\sqrt{s}=91\,\mathrm{GeV}$ are consistent [14], so the mixture of charmed hadrons produced in $Z^0\to c\bar{c}$, $g\to c\bar{c}$, and in b hadron decays were taken from Reference [14], as were the semileptonic branching ratios of charm hadrons. All samples were processed with the OPAL detector simulation package [15].

[1] Charge conjugation is assumed throughout this paper.

3 Jet selection

3.1 Jet reconstruction

Measurement of secondary charm pair production could in principle be reduced to a charm hadron counting experiment in events where the primary quarks were light flavoured, i.e. up, down, or strange quarks. However, such a sample is hard to obtain as $Z^0\to c\bar{c}$ and $Z^0\to b\bar{b}$ events can not be identified with 100 % efficiency. Instead, by grouping the particles of an event into jets, charmed hadrons which are produced from the primary quarks can more easily be identified and counted as background.

To identify the process of gluon splitting into a charm-quark pair, we required the event to contain exactly three jets. Using simulated events, we investigated the effect of various jet finding algorithms to select the three-jet topology. Of the Durham, Geneva, Cone, and JADE-E0 algorithms [16] that were tested, the JADE-E0 recombination scheme with a y_{cut} value of 0.05 gave the most significant $g\to c\bar{c}$ signal. As can be seen from Fig. 1a, the two secondary charm quarks tend to be contained within a single jet, so that in three-jet events, $g\to c\bar{c}$ events were identified more efficiently than background events.

For the selected three-jet events, the jet energies were calculated, neglecting mass effects, using the relation

$$E_i = E_{\mathrm{cm}}\frac{\sin\psi_{jk}}{\sin\psi_{jk}+\sin\psi_{ij}+\sin\psi_{ik}}, \qquad (2)$$

where E_{cm} is the center-of-mass energy, ψ_{ij} is the angle between jets i and j and E_i is the calculated energy of jet i. This equation only holds for coplanar events and therefore, if the sum of the angles between the jets was smaller than 358°, the event was rejected. These criteria retain 30 % of the data sample. From the simulation, the efficiency for $g\to c\bar{c}$ events to pass the selection is 56 %.

In the previous OPAL analysis [6], only 3.5 million hadronic Z^0 decays were used, with a y_{cut} value of 0.03, compared to 4.4 million events and a y_{cut} value of 0.05 used here.

3.2 Gluon jet selection

The gluon jet candidate in the event was then selected. Several selection algorithms were tried, of which two were retained, based on their efficiency for selecting the correct jet and for background rejection. The first method, already used in Reference [6], assumes that the lowest energy (LE) jet is the gluon jet. The second method, used here for the first time, takes the jet that is most readily subdivided into two as the gluon jet candidate (JS), and was found to correctly identify the gluon jet in $g\to c\bar{c}$ events more often. This method is motivated by the fact that the gluon jets of

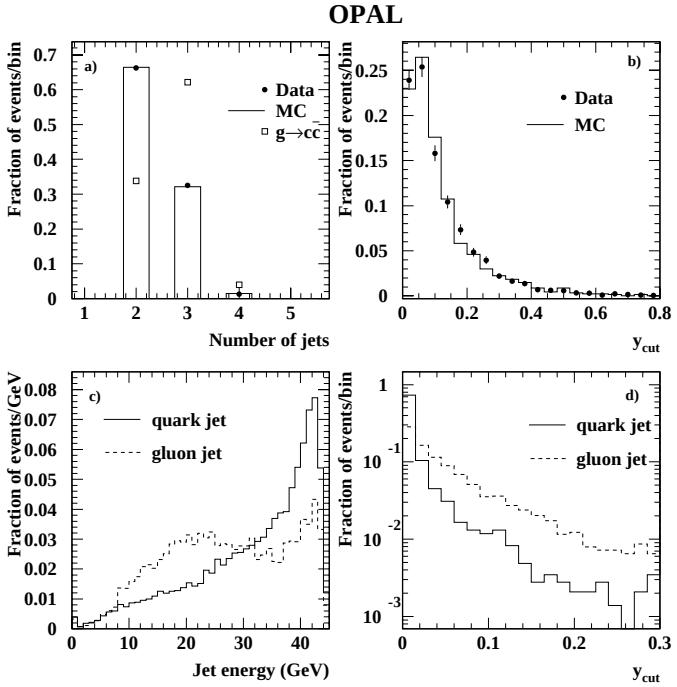

Fig. 1a–d. Jet selection properties: **a** number of jets in the events; **b** y_{cut} value where a selected jet splits into two subjets for all three-jet events; **c** jet energy for quark and gluon jets in Monte Carlo g→c$\bar{c}$events; **d** y_{cut} value at the point where a jet splits into two subjets for quark and gluon jets. The Monte Carlo histograms in **a** and **b** include the default JETSET value of $g_{c\bar{c}}$=0.014

interest contain two charmed hadrons, and should therefore show more evidence of jet substructure than primary charm jets and most bottom jets which contain only one charmed hadron. The JADE-E0 jet finding algorithm was applied to each jet individually, and the gluon jet candidate is taken to be the one with the highest value of y_{cut} at which the jet splits into two subjets. Using the new JS method, the correct gluon jet is identified in 60 % of three-jet events from the signal process g→c$\bar{c}$, while the corresponding number for the LE method is 51 %.

The performance of the two gluon selection schemes was investigated for both the lepton and the $D^{\star\pm}$ analyses. The LE method performed better than the JS method for the lepton analysis, after all the additional background rejection criteria had been applied (Sect. 4.2). The overall efficiency of the lepton analysis using the LE method was 66 % of the efficiency using the JS method, but with a factor of three less background from primary heavy-quark events, yielding a 15% advantage in statistical significance. In contrast, for the $D^{\star\pm}$ analysis, the JS method outperformed the LE method; the efficiency for the $D^{\star\pm}$ analysis doubled when using the JS method while the heavy quark background only increased by a quarter, yielding an improvement in statistical significance of 80%. As a results of these studies, the LE method was used for the lepton analysis while the JS method was used for the $D^{\star\pm}$ analysis.

Figure 1b shows the y_{cut} value of the selected jet at the point where that jet splits into two subjets, for all three-jet events selected from data and the Monte Carlo simulation. Figure 1c shows the distribution of the jet energy for quark and gluon jets from the process g→c$\bar{c}$, and Fig. 1d shows the y_{cut} value at the jet splitting point for these jets.

4 The lepton analysis

Using the sample of three-jet events, and taking the gluon jet candidate to be the lowest energy jet (LE method), events containing the gluon splitting process, g→c$\bar{c}$, were searched for using a lepton tag, which assumes that one of the charm quarks decayed semi-leptonically.

4.1 Lepton identification

Electrons were identified using an artificial neural network [17] while muons were identified using information from the muon chambers in association with the tracking chambers, as in [18]. The lepton identification was limited in polar angle θ, defined as the angle between the lepton candidate and the beam axis direction of outward-going electrons. The polar angle of identified electrons was limited to $|\cos\theta| < 0.8$, while identified muons were required to be within $|\cos\theta| < 0.9$. In addition, the momentum of the lepton candidate was required to satisfy $2 < p < 9\,\mathrm{GeV}/c$, and have a transverse momentum, with respect to the jet axis containing the candidate, below $2.75\,\mathrm{GeV}/c$. Electrons consistent with being produced from photon conversions or from Dalitz decays were rejected with an artificial neural network using geometrical and kinematical properties [17].

The efficiency for leptons from the g→c$\bar{c}$ signal events to pass the lepton identification and the momentum selection criteria was 16 % for electrons, and 17 % for muons. This differs from the previous OPAL analysis [6], with the most significant difference being the larger momentum range used. Previously muons were only accepted in the narrower range of $3 < p < 6\,\mathrm{GeV}/c$. The shift to the larger momentum range, together with the improvements in electron identification and the photon conversion finder, have resulted in a larger efficiency for identifying leptons from g→c$\bar{c}$.

At this point, the data sample contained 7 180 tagged electron candidates and 14 631 tagged muon candidates, corresponding to a $g_{c\bar{c}}$ purity of 10 % and 6 % respectively, while the efficiency to detect a lepton from the g→c$\bar{c}$ process that passes all the criteria described above (Sects. 2-4.1) was approximately 7.5 %. The large difference between the number of selected electrons and muons is mostly due to contamination of hadrons passing the muon selection criteria, as described in Sect. 4.3.

4.2 Suppression of jet mis-assignment background

With the selection of lepton tagged events described above, background contributions from events with jet mis-assignment were unavoidable: Jet mis-assignment events are defined as those where the lowest energy jet contains a lepton from the decay of a primary heavy quark rather than from a heavy quark in a gluon jet. The jet mis-assignment background is dominated by $Z^0 \to b\bar{b}$ events, and was suppressed by means of a b-tagging algorithm based on reconstructed displaced secondary vertices. A neural network with inputs based on decay length significance, vertex multiplicity and invariant mass information [19] was used to select vertices with a high probability of coming from b hadron decays. Events were rejected if any of the three jets were tagged by the neural network. This procedure resulted in a reduction of the jet mis-assignment background by 43 %, which included a 54 % reduction in $b\bar{b}$ events, while retaining 78 % of the $g \to c\bar{c}$ sample. After this cut the data sample contained 5 049 electron candidates and 11 031 muon candidates.

To further reduce the jet mis-assignment background from non-gluon jets, we explored several properties of the lowest energy jet, with respect to the other two. Naively, as a jet containing the gluon splitting $g \to c\bar{c}$ contains two charm quarks, one would expect the jet mass and multiplicity to be larger for that jet than for the other two jets. Comparison of Monte Carlo samples containing the signal, with samples of $Z^0 \to b\bar{b}$ and $Z^0 \to c\bar{c}$ events in which a lepton coming from the decay of a primary b or c quark was assigned by the jet finder to the lowest energy jet showed that background rejection through mass and multiplicity cuts was indeed feasible, and the following requirements were found to give the best background rejection:

- $\mathrm{M}ax(M_1, M_2)/\mathrm{M}_3 < 2$, where M_i is the mass of the ith jet, and the jets are ordered by energy, with jet 1 having the highest energy.
- $(N_1 + N_2)/\mathrm{N}_3 < 2.5$, where N_i is the track and electromagnetic cluster multiplicity of the ith jet, where an electromagnetic cluster was counted only if no charged track was associated with it.

These two selection criteria retained 55 % of the $g \to c\bar{c}$ events, while rejecting 71 % of the $Z^0 \to c\bar{c}$ background and 67 % of the $Z^0 \to b\bar{b}$ background. On application of the jet mis-assignment background suppression, in conjunction with the lepton tagging selection criteria described previously, and accepting only one lepton tag candidate in each event (with priority given to electrons due to the higher muon fake rate), the data sample was reduced to 2 434 electron candidate events and 4 362 muon candidate events. At this stage, no further background suppression was done. Rather, the remaining backgrounds in the data sample were evaluated using Monte Carlo estimates (see Sect. 4.3).

4.3 Estimates of background rates

The determination of the rate of each background source is discussed below. A summary of the estimated data sample composition is given in Table 1.

Jet mis-assignment background

The rate of the jet mis-assignment background was estimated from the 14.5 million hadronic Z^0 decays of the Monte Carlo sample mentioned in Sect. 2, after applying all the selection cuts of Sect. 4.2. The number of leptons from semileptonic decays of charm and bottom hadrons was determined, excluding leptons from $g \to c\bar{c}$ or $g \to b\bar{b}$ decays. By scaling to the number of hadronic events in the data sample, we estimated this background to contain 1 027±32 candidates from $Z^0 \to b\bar{b}$ events and 702±26 candidates from $Z^0 \to c\bar{c}$ events, where these uncertainties are statistical only.

Photon conversions

From the Monte Carlo simulation, the photon conversion finder fails to tag (14.3±0.4) % of the conversions, where the uncertainty is from the systematic uncertainties in the conversion finding efficiency [17]. These untagged conversion electrons then form a background to the electron tagged events. Knowing the efficiency of the conversion finder, the background from untagged conversions was estimated from the number of tagged conversions to be 630±25 events.

Lepton mis-identification and decays in flight

To estimate the background from hadrons which were erroneously identified as lepton candidates, we used the Monte Carlo sample to determine the probability that a charged track with a given momentum, p, and transverse momentum with respect to the direction of the associated jet, p_t, should be incorrectly identified as a lepton. The number of background leptons in the data was then derived by multiplying the number of tracks in the data that passed the selection criteria, excluding the lepton identification, by these fake probabilities. In practice the fake probabilities per track are estimated in bins of p and p_t, and corrected for differences between the Monte Carlo simulation and the data, as in [18]. The correction for the difference between the MC and the data introduces a large uncertainty on the number of hadrons mis-identified as leptons as described in Sect. 6.1

The total number of hadrons mis-identified as muons was estimated at 2 580±51. Decays in flight of light hadrons into muons are included in this estimate. The number of hadrons mis-identified as electrons was estimated by a similar method to be 81±9.

Table 1. Summary of selected sample sizes and estimated composition. The second error in the estimated signal row represents the Monte Carlo statistical error

Quantity	Electron channel	Muon channel
Observed events	2 434	4 362
Jet mis-assignment ($c\bar{c}$)	342±19	360±18
Jet mis-assignment ($b\bar{b}$)	494±22	533±23
Residual photon conversion	630±25	-
Lepton mis-identification	81±9	2 580±51
Dalitz decays	149±12	-
$g \to b\bar{b}$	50±7	53±7
Estimated signal	688±42±16	836±59±13

Dalitz decays of π^0 and η

The number of background events from the decay of π^0 and η into $e^+e^-\gamma$ was estimated from Monte Carlo simulation and corrected to the known π^0 and η multiplicities in Z^0 decays [14]. These contributions were estimated at 149±12 electron candidate events.

Gluon splitting: $g \to b\bar{b}$

The number of events from the process $g \to b\bar{b}$ that survive the selection criteria was calculated from $g_{b\bar{b}} \cdot N_{had} \cdot \epsilon^b$, where ϵ^b is the efficiency for at least one lepton from the process $g \to b\bar{b}$ to survive the selection criteria, N_{had} is the number of hadronic events, and $g_{b\bar{b}} = (2.69 \pm 0.67) \times 10^{-3}$ is the averaged measured value of $g_{b\bar{b}}$ taken from [13]. From Monte Carlo simulation, ϵ^b was found to be (1.0 ± 0.1) %, leading to an estimated background of 103±10.

4.4 Comparison of the data and Monte Carlo

Since a major part of the background contribution has been estimated from the Monte Carlo, it was crucial that the consistency between the Monte Carlo and the OPAL data be verified. Of particular importance was the accuracy in the simulation and estimation of the jet mis-assignment background, as the efficiency to tag a heavy quark jet as a $g \to c\bar{c}$ and the fraction of heavy quark jets found in the lowest energy jet were critical to this analysis.

To check the validity of the jet mis-assignment background composition, we examined the lepton yield in three-jet events where the lepton did not originate from the lowest energy jet. Specifically, we searched for events with leptons in either of the two highest energy jets which passed all but the lepton requirement in the third jet of the selection criteria. The leptons were identified using the same criteria as described in Sect. 4.1, and the jet-based mass and multiplicity cuts were applied in the same fashion as in Sect. 4.2. However, the search was restricted to prompt leptons from b hadron decay by requiring lepton momenta above 5 GeV/c and transverse momenta above 1.5 GeV/c. The resulting yield of such leptons per three-jet event was found to be $(1.49 \pm 0.02) \times 10^{-3}$ in the Monte Carlo and $(1.47 \pm 0.02) \times 10^{-3}$ in the data. For the Monte Carlo sample the simulation showed that the b-hadron purity of these events was 85 %.

We also looked at events tagged as $Z^0 \to b\bar{b}$ with the b-tagging algorithm described in Sect. 4.2 in order to compare the jet mis-assignment rate in $Z^0 \to b\bar{b}$ events. This was done by searching for a lepton in the lowest energy jet of events that have vertices compatible with b-hadron decay. After applying all other selection criteria we observed 646 such events in the data. The Monte Carlo prediction scaled to the data sample size was found to be 632 events. The Monte Carlo simulation estimated that the b hadron purity of these events was approximately 93 %. From the agreement of the Monte Carlo prediction with the data sample estimates for these two tests, the data/Monte Carlo consistency was found to be adequate, and the jet mis-assignment well modelled in the Monte Carlo.

In addition, comparisons of the Monte Carlo simulation prediction and data distributions for the variables critical to the lepton tagging analysis were made, with the results of the comparison shown in Fig. 2. Specifically, Fig. 2a shows the ratio of the maximum mass of the first two jets with respect to the third jet. Figure 2b shows the ratio of the multiplicity of tracks and unassociated clusters in the first two jets with respect to the third jet. Figure 2c shows the lepton candidate momentum spectrum for events passing all the selection criteria, and 2d shows the lepton candidate transverse momentum. All plots present the Monte Carlo prediction which include the $g \to c\bar{c}$ contribution normalised to the number of signal events obtained in this analysis. This comparison shows an agreement between Monte Carlo and data in both shape and rate prediction. Thus, the procedure of subtracting the Monte Carlo prediction for the jet mis-assignment background was justified.

4.5 Results

The charm-quark-pair production rate per hadronic event is related to the measured quantities by

$$g_{c\bar{c}} = \frac{N_{sel}}{N_{had} \cdot \epsilon \cdot 2 \cdot B(c \to X\ell\nu)}, \qquad (3)$$

where the following notation is used; N_{sel} is the number of events passing the selection criteria after subtraction of background events (Table 1), N_{had} is the number of hadronic Z^0 decays, ϵ is the efficiency for finding a single lepton from a sample of $g \to c\bar{c}$ Monte Carlo events in which at least one of the charmed hadrons decayed semileptonically and passed the selection criteria, and $B(c \to X\ell\nu)$ is the charm hadron semileptonic branching ratio of (9.5 ± 0.7) % obtained by taking the average of the most recent measurements of OPAL[20] and ARGUS[21]. With $N^e_{sel} = 688 \pm 42$, $N^\mu_{sel} = 836 \pm 59$,

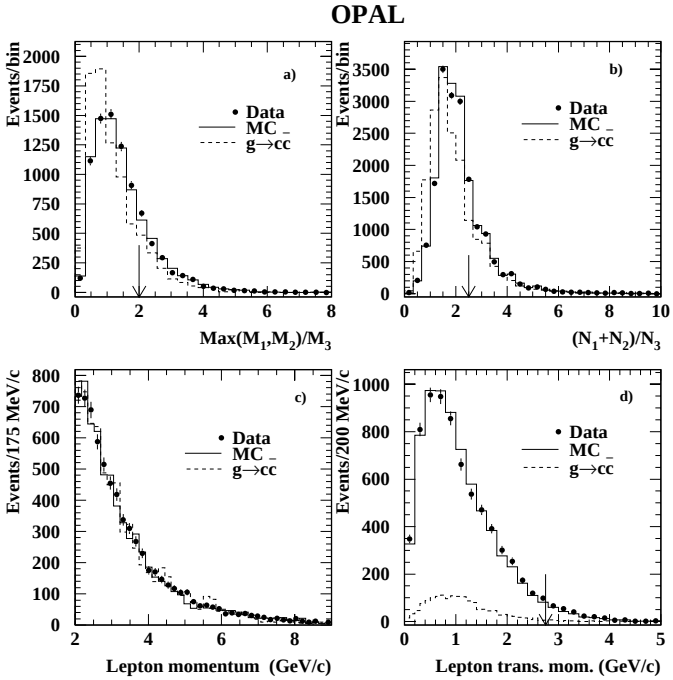

Fig. 2a–d. Comparison of data and Monte Carlo for the lepton analysis (histograms represent the Monte Carlo and data are represented by the points, the dashed histograms show the g→c$\bar{c}$ spectrum). Monte Carlo distributions (solid and dashed histograms) are normalised to the number of hadronic events in the data. **a** Ratio of the maximum mass of the first two jets with respect to the third jet for events that passed the lepton selection and the b-tagging neural network rejection; **b** ratio of the multiplicity of tracks and unassociated clusters in the first two jets with respect to the third jet for the events in **a**; **c** lepton candidate spectrum for events passing all the selection criteria; **d** lepton candidate transverse momentum spectrum for events passing all but the transverse momentum criteria with the g→c$\bar{c}$ spectrum scaled to the signal area. The arrows in **a**, **b** and **d** show the cut value used in this analysis. Events below these values were accepted

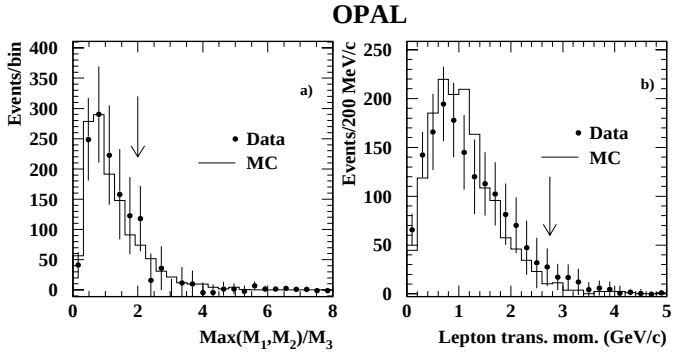

Fig. 3a,b. Distributions of **a** $Max(M_1, M_2)/M_3$, **b** lepton transverse momentum for background subtracted data (points) and for g→c$\bar{c}$ Monte Carlo scaled to the average lepton analysis $g_{c\bar{c}}$ result (solid line): All the selection criteria described in the text were applied with the exception of the variable in each plot where the cut is shown by the arrow. The error bars shown represent the statistical and systematical uncertainties combined

$\epsilon^{e} = (2.72 \pm 0.12)\,\%$ and $\epsilon^{\mu} = (2.83 \pm 0.13)\,\%$ we obtained

$$g^{e}_{c\bar{c}} = 0.0303 \pm 0.0028, \quad (4)$$

$$g^{\mu}_{c\bar{c}} = 0.0353 \pm 0.0037, \quad (5)$$

where the uncertainties are the statistical contributions only. Figure 3a gives the comparison between the background subtracted data distribution of the three-jet mass variable, and the JETSET prediction for the same distribution (normalised to the data sample). A clear enhancement in the mass distribution is visible at low values of the mass ratio, which is well described by the Monte Carlo prediction, and when compared to Fig. 2a, justifies the cut used in Sect. 4.2. Furthermore, the agreement between data and Monte Carlo suggests that JETSET describes the production and shape of secondary heavy quarks rather well. Figure 3b shows the spectrum of the lepton transverse momentum for the background subtracted data and for the g→c$\bar{c}$ Monte Carlo simulation scaled to the data size. Here too, a reasonable agreement between the data and Monte Carlo is seen. Leptons were accepted if their transverse momentum was smaller than 2.75 GeV/c (where the majority of the signal was found).

5 The $D^{\star\pm}$ analysis

As $D^{\star\pm}$ mesons are copiously produced from charm quarks and have a clear signature, they can be used to tag charmed hadrons in a gluon jet. Using the three-jet event sample, we chose the gluon jet candidate using the jet splitting technique described in Sect. 3.2, and searched for a $D^{\star\pm}$ meson in this jet. The $D^{\star+}\to D^0\pi^+$, $D^0 \to K^-\pi^+$ decay channel gives a clean signal, since the small mass difference between the $D^{\star\pm}$ and the D^0 limits the phase space available, reducing combinatorial background.

The D^0 reconstruction was performed as in [5] by trying all combinations of oppositely charged tracks, assuming one of them to be the kaon, and the other to be the pion. We then added a third track, the "slow pion", demanding its charge to be equal to that of the pion candidate track, to form the $D^{\star\pm}$ candidate.

The following mass cuts were applied:

- The reconstructed D^0 mass must lie within 75 MeV of the nominal D^0 mass.
- The mass difference, ΔM, between the $D^{\star\pm}$ and the D^0 candidates must be in the range $0.143\,\mathrm{GeV}/c^2 < \Delta M < 0.147\ \mathrm{GeV}/c^2$.

To further reduce the background from random combinations, the following criteria were imposed:

- The measured rate of energy loss for the kaon candidate track was required to be consistent with that expected for a kaon with a probability of more than 0.1.

Table 2. Summary of observed events and estimated background for the $D^{\star\pm}$ analysis

Observed events	308
Combinatorial background	171.1±13.1
Jet mis-assignment ($b\bar{b}$)	19.2±4.3
Jet mis-assignment ($c\bar{c}$)	35.9±6.0
$g \to b\bar{b}$	4.0±2.0
Estimated signal	77.8±15.2

- The kaon candidate track momentum satisfied $p_K > 1.5\,\mathrm{GeV}/c$.
- The ratio between the measured $D^{\star\pm}$ energy to the total energy measured in the selected jet satisfied $X_{jet} = \frac{E_{D^*}}{E_{jet}} > 0.2$.
- The helicity angle, θ^*, measured between the kaon in the D^0 rest frame and the D^0 direction in the laboratory frame satisfied $\cos\theta^* < 0.7$. The D^0 decays isotropically in its rest frame creating a flat distribution of $\cos\theta^*$, while background events are peaked at $\cos\theta^* = 1$.

Charmed hadrons which pass these selection criteria can also be produced in b hadrons decays. The artificial neural network described in Sect. 4.2 was used to reject such events.

Applying all these selection criteria reduced the three-jet data sample from 1.32 million events to 308 events. This large reduction in sample size is partially due to the low branching ratio of the decay chain as well as the result of the background suppression criteria. The shape of the remaining combinatorial background was described by a function of the form $(\Delta M - 0.139)^a(b + c\Delta M + d(\Delta M)^2)$, with a, b, c, and d determined from the sideband of the D^0 mass distribution with the signal being found in the 2.16 GeV/c^2< $M_{K^-\pi^+}$ < 2.46 GeV/c^2 region. The normalisation of the background was determined outside the signal region. The estimated background in the signal region was estimated to be 171.1±13.1 events. The distribution of ΔM is shown in Fig. 4a where a significant signal above the fitted background estimation is observed around 145 MeV/c^2.

The jet mis-assignment background was estimated from the Monte Carlo simulation as in 4.3. We estimated this background to be 35.9±6.0 and 19.2±4.3 events from $c\bar{c}$ and $b\bar{b}$ events respectively.

The remaining source of background considered was from secondary b quark pair production ($g \to b\bar{b}$). To estimate its contribution, an average value of $g_{b\bar{b}} = (2.69 \pm 0.67) \times 10^{-3}$ [13] was used, along with a selection efficiency of 0.034 % (including branching ratios), resulting in a $g \to b\bar{b}$ background estimate of 4.0±2.0 events. A summary of the sample composition is given in Table 2.

In a similar fashion to Sect. 4.4, we have compared the Monte Carlo simulation with the data. Figure 4b shows the ratio of the $D^{\star\pm}$ candidate energy to the jet energy for candidates in the selected gluon jet after applying the combinatorial rejection criteria. The Monte Carlo distribution contains a $g \to c\bar{c}$ component scaled to the result obtained for this channel ($g_{c\bar{c}} = 0.04$).

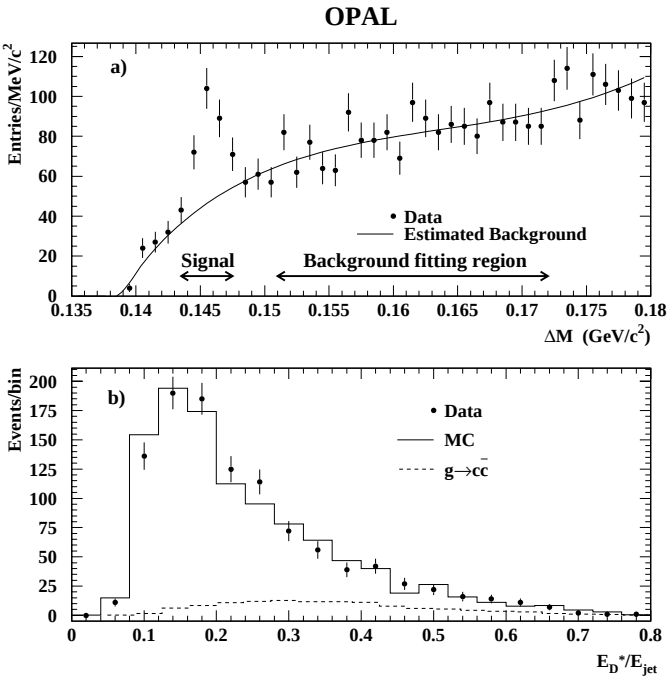

Fig. 4a,b. a The distribution of the difference of the invariant mass between the $D^{\star\pm}$ candidate and the D^0 candidate, ΔM. The solid curve represents the estimated background shape. An estimated 137±13 $D^{\star\pm}$ candidates are above the background fit around 0.145 GeV/c^2. **b** Ratio of the $D^{\star\pm}$ candidate energy to the jet energy for candidates in the selected gluon jet after applying the combinatorial rejection criteria. The solid line shows the Monte Carlo spectrum with the $g \to c\bar{c}$ component scaled to measured value in the $D^{\star\pm}$ analysis ($g_{c\bar{c}}$=0.04), and the dashed histogram shows the spectrum for true $D^{\star\pm}$ mesons from $g \to c\bar{c}$ scaled to the measurement area

To obtain the rate of $g \to c\bar{c}$ we modified equation 3 to account for the $c \to D^{\star\pm}$, $D^{\star\pm} \to D^0\pi^+$and $D^0 \to K^-\pi^+$ branching ratios. The product of the first two was taken to be (15.27±0.92) % [13] and $B(D^0 \to K^-\pi^+)$ to be (3.85±0.09) % [14]. The number of selected events was $N_{sel} = 77.8 \pm 15.2$, and the selection efficiency found from the Monte Carlo was $\epsilon = (3.70 \pm 0.12)$ %. This gives

$$g_{c\bar{c}} = 0.0408 \pm 0.0122, \tag{6}$$

where the uncertainty is statistical.

6 Systematic uncertainties

Possible sources of systematic uncertainty and their effect on the background and efficiency are discussed below. The systematic uncertainties on $g_{c\bar{c}}$ from the different sources are summarized in Table 3 separately for the electron, muon and $D^{\star\pm}$ measurements.

6.1 Lepton identification

Muon identification efficiency: The systematic uncertainty from the muon identification efficiency was evaluated using a method similar to that in Reference [18]. The muon identification efficiency was compared in data and Monte Carlo using various control samples, including $Z^0 \to \mu^+\mu^-$ events, and muons reconstructed in jets. Without using dE/dx information, an uncertainty of $\pm 2.0\,\%$ was found.

However, as dE/dx information is an important input to muon identification, the effect of mis-modelling of the dE/dx was studied. The mean dE/dx for muons in $Z^0 \to \mu^+\mu^-$ events was observed to be shifted by approximately 15 % of the dE/dx resolution with respect to the theoretically expected value. A similar shift was observed in the Monte Carlo simulation, both for muon pairs and for muons identified inclusively in jets, and an uncertainty on the modelling of the dE/dx mean of $\pm 5\,\%$ was assigned. The dE/dx resolution was studied in the data and Monte Carlo using test samples and was found to be modelled to better than 5 %. The uncertainties on these sources gave a total uncertainty on the efficiency of muon identification of $\pm 3.0\,\%$.

Muon mis-identification rate: There was an uncertainty on the number of hadrons that were incorrectly identified as muons. This predominantly arises from uncertainties in the simulation of the fake probabilities. Three samples were used to test the Monte Carlo modelling of these probabilities:

- pions from identified $K^0_s \to \pi^+\pi^-$ decays. The Monte Carlo predicted that the tracks in this sample were more than 99 % charged pions with less than 0.1 % contamination from prompt muons.
- three-prong τ decays. The Monte Carlo predicted that the tracks in this sample were more than 99 % charged pions with less than 0.1 % contamination from prompt muons.
- a sample of tracks passing a set of dE/dx requirements designed to enhance the fraction of charged kaons.

These samples were obtained and used as in Reference [18] to obtain the fake rate uncertainty for identified muons from semileptonic decays in $Z^0 \to b\bar{b}$ and $Z^0 \to c\bar{c}$ events. This gave a multiplicative correction to the Monte Carlo simulation fake rate probability of 1.09 ± 0.10. The uncertainty on the correction factor strongly depends on the particle composition of the hadron sample.

This procedure was repeated for the lower momentum spectrum and the particle composition applicable for this analysis to give a correction factor of 1.09 ± 0.06. As the fraction of pions in this analysis is larger than in [18], the contribution of the relatively large uncertainty associated with the charged kaon sample becomes smaller and the overall uncertainty on the fake probability is reduced. Hence, the systematic uncertainty on the number of hadrons that were mis-identified as muons is 154 events.

Electron identification efficiency: The uncertainty on the simulated electron identification efficiency was taken from Reference [17]. This study is summarised below.

The most important variables that were used in the electron identification neural network were the specific energy loss dE/dx, its error, and the ratio of the track's energy deposited in the calorimeter to the track's momentum. The Monte Carlo simulation and data distributions of these variables were compared using samples of identified particles.

The dE/dx measurements were calibrated in data using samples of inclusive pions at low momenta and electrons at 45 GeV/c from Bhabha events. The quality of the calibration was checked with control samples, the most important of which were pions from K^0_s decays and electrons from photons converting in the detector. There was a smaller than 5 % difference between the mean dE/dx measured in these samples in the data, and the corresponding sample in the Monte Carlo simulation. Similarly, the dE/dx resolution in these samples have been studied and the data and Monte Carlo simulation were found to agree to within 8 %. The uncertainty on the electron identification efficiency from these two sources was found by varying both simultaneously, and was $\pm 2.5\,\%$

A similar study has been performed for the next most significant input variable E/p, which has a resolution in the Monte Carlo around 10 % worse than in the data. To correct for this the Monte Carlo has been reweighted to match the data, resulting in a variation of the efficiency of $\pm 2.7\,\%$.

No significant contribution to the electron efficiency uncertainty was found from the other input variables. The uncertainty arising from them was estimated from the statistical precision of these tests, which was less than 1 % of the efficiency. In total, an uncertainty of $\pm 4.0\,\%$ was assigned to the electron identification efficiency.

Electron mis-identification rate: The uncertainty on the simulated electron fake rate was evaluated as in [17]. The study used $K^0_s \to \pi^+\pi^-$ decays and three-prong τ decays, and gave a fake rate uncertainty of 21 % which corresponds to 17 events.

Photon conversion tagging efficiency: The uncertainty on the modelling of the photon conversion tagging efficiency was estimated by comparing data and Monte Carlo samples of identified electrons with low momentum and low transverse momentum. These samples had a very high electron purity and a photon conversion purity of 77 %. The uncertainty on the photon conversion tagging efficiency was estimated to be 3.5 % giving a systematic uncertainty of 27 events.

Dalitz decays: The uncertainty from this source arises from the modelling of the efficiency and from the limited knowledge of the π^0 and η multiplicities. A systematic uncertainty was assigned for possible differences between the multiplicity of neutral pions and η mesons in the Monte Carlo simulation and data. The production rates

in the Monte Carlo were varied within the experimental uncertainties on the measured multiplicities [14], giving a 1.2 % uncertainty on the electron channel result. Combining these sources of uncertainty, we estimated the uncertainty on the number of events from Dalitz decays to be 13 events.

Lepton transverse momentum: To estimate the effect of the lepton transverse momentum criterion on the efficiency we compared the fraction of events that pass this criterion in data and in the Monte Carlo simulation. We found this effect to be of the order of 1.3%.

6.2 $D^{\star\pm}$ identification

$D^{\star\pm}$ reconstruction efficiency: As the efficiency to reconstruct a $D^{\star\pm}$ was found to be smaller for low $D^{\star\pm}$ momentum, the compatibility of the data and the Monte Carlo $D^{\star\pm}$ reconstruction efficiency was compared by studying the ratio of the $D^{\star\pm}$ yield in Monte Carlo and data in different momentum regions. Since no significant difference between low and high momentum regions was observed, the statistical precision of this test was assigned as the systematic uncertainty. The mis-modelling of ΔM resolution was also studied. The observed difference in ΔM width between the data and Monte Carlo was found to be $0.15\,\mathrm{MeV}/c^2$ resulting in a 2.3 % uncertainty on the $D^{\star\pm}$ efficiency. The uncertainty arising from the modelling of $\mathrm{d}E/\mathrm{d}x$ was estimated by comparing the selection to a modified version, where no $\mathrm{d}E/\mathrm{d}x$ requirements where made. The change in the yield in the Monte Carlo and data was consistent. The 3.2 % statistical precision of this test was assigned as the uncertainty from this source. Combining these effects, we obtained a 4.2 % uncertainty on the $D^{\star\pm}$ efficiency.

$D^{\star\pm}$ background modelling: The background fitting procedure was repeated changing the region of ΔM used for the normalisation. In addition we also changed the D^0 mass sideband to include the lower sideband ($1.26\ \mathrm{GeV}/c^2 < \mathrm{M}_{K^-\pi^+} < 1.56\ \mathrm{GeV}/c^2$). A different parametrisation for the background shape was also tried and the result was consistent with that of the original parametrisation. As the uncertainty arising from the alternative parametrisation was smaller than that of the original parametrisation, we took the latter as the uncertainty associated with the background shape parametrisation. Adding the differences due to the above tests, and due to the uncertainties on the fitting parameters, we obtained an uncertainty of 3.3 % on the number of $D^{\star\pm}$ mesons.

6.3 QCD and fragmentation

Secondary charm production modelling: As there are no measurements of the momentum spectrum of charmed hadrons from the process of $g\to c\bar{c}$ to test the modelling, the JETSET parameters with which the events were generated were varied according to Reference [22]. The parton shower Λ value was varied in the range 0.13 to 0.31 GeV. The invariant mass cut-off of the parton shower Q_0 was varied between 1.4 and 2.5 GeV. The parameter σ_q, the width of the primary hadrons transverse momentum distribution was varied in the range 0.37 to 0.43 GeV and b, the parameter of the Lund symmetric fragmentation function was varied in the range 0.48 to $0.56\,\mathrm{GeV}^{-2}$. Full detector simulation was not available for all these variations of the model parameters, and therefore, estimates of their effect were made by applying appropriate cuts and smearing the event properties. In addition we have compared HERWIG [23] and ARIADNE [24] to JETSET. We have taken the largest difference between the three predictions as an extra source of uncertainty.

Fragmentation modelling: The heavy-quark fragmentation was simulated using the function of Peterson et al.[12] and light-quark fragmentation was simulated according to the Lund symmetric scheme. The heavy-quark fragmentation model parameters were varied to change the mean scaled energy of weakly-decaying bottom and charm hadrons within their experimental range: $\langle x_E\rangle_\mathrm{b} = 0.702\pm0.008$ and $\langle x_E\rangle_\mathrm{c} = 0.484\pm0.008$ respectively [13]. In addition, the heavy-quark model was changed to the Lund symmetric model, to that suggested by Collins and Spiller [25] and to that of Kartvelishvili et al.[26] with parameters tuned according to Reference [27]. The largest difference between the Peterson fragmentation and the other models was taken as a systematic uncertainty.

Jet scheme dependence: The stability of the results has been checked by changing the jet finding algorithm to the Durham scheme, with y_cut set to $y_\mathrm{cut} = 0.015$; this choice of y_cut value was made as it optimised the significance of the observed signal. With this value, we obtained $\mathrm{g}^\mathrm{e}_{c\bar{c}} = 0.0330 \pm 0.0032$ and $\mathrm{g}^{\mu}_{c\bar{c}} = 0.0401 \pm 0.0043$ for the electron and muon channels respectively (here the uncertainties are statistical only). The slightly larger statistical uncertainties with respect to the Jade jet finding results (equations 4 and 5) justify the choice of the Jade algorithm for this analysis. Considering the 57 % overlap of the Jade and Durham samples, the two results are consistent and no additional systematic uncertainty was introduced.

6.4 Heavy quark production and decay

Semileptonic decay modelling (lepton channels only): Events with a prompt lepton were reweighted as a function of the lepton momentum in the rest frame of the decaying heavy hadron to simulate different models of semileptonic decay as in [13]. The semileptonic decay model of Altarelli et al.[28] (ACCMM), with parameters tuned to CLEO data [29] for b decays and to DELCO [30] and MARK III [31] data for charm decays, was used for the central values, and was combined with the $\mathrm{b}\to\mathrm{D}$ spectrum measured by CLEO [32] for $\mathrm{b}\to\mathrm{c}\to\ell$ decays. The model of Isgur et al.[33] (ISGW) and their modified model (ISGW**) with the fraction of $D^{\star\star}$ decays determined from CLEO data [29] were used to determine the

systematic uncertainty due to the $b \to \ell$ spectrum.

Charm and bottom branching ratios: The dependence on the semileptonic branching ratios, $b \to \ell$, $c \to \ell$, $b \to c \to \ell$, as well as the hadronic branching ratios of $b \to D^{\star\pm}$, $c \to D^{\star\pm}$, $D^{\star+} \to D^0\pi^+$ and $D^0 \to K^-\pi^+$, has been investigated by varying them within their experimental uncertainties [14,13,21,20].

A possible energy dependence of the $B(c \to D^{\star\pm}) \times B(D^{\star\pm} \to D^0\pi)$ rate has been taken into account by comparing the average of LEP measurements, 0.1527 ± 0.0092 [13], with an average of lower energy measurements, 0.184 ± 0.014 [14]. Typical $D^{\star\pm}$ energies in this analysis were between these extremes, and the uncertainty on this product branching ratio has been inflated to 0.015 to account for these possible effects. In contrast, the OPAL and ARGUS [20,21] values for the semileptonic branching ratio $c \to \ell$ are consistent, and no additional uncertainty has been assigned.

Partial hadronic widths: The partial hadronic widths of bottom and charm with which both the efficiency and the jet mis-assignment background were estimated, were taken from a combination of LEP and SLD results [13]. The error on the partial widths is a source of systematic uncertainty on $g_{c\bar{c}}$

$g \to b\bar{b}$: The uncertainty on the average measured value of $g_{b\bar{b}}$ gave an uncertainty of 14, 15, and 1.1 events on the number of background events for the electron, muon, and $D^{\star\pm}$ channels respectively.

Jet mis-assignment background modelling: This background could be mis-modelled if the efficiency for tagging a heavy quark jet was incorrect, or if the fraction of primary heavy quark jets which were identified as the gluon jet candidates was mis-modelled in the Monte Carlo. We tested these cases, using enriched $Z^0 \to b\bar{b}$ samples (as described in Sect. 4.4), As data and Monte Carlo were consistent in all cases we assigned the statistical precision of these tests as a systematic uncertainty. We assigned the difference solely to the signal, using the test purity, and took the larger difference as a systematic uncertainty.

Jet mass criterion: The systematic uncertainty associated with the jet mass criterion was found by comparing the fraction of events passing this selection in data and Monte Carlo. The systematic uncertainty assigned to this source is 2.3%.

B hadron decay product multiplicity: The artificial neural network used to reject $Z^0 \to b\bar{b}$ events was sensitive to the B hadron charged track multiplicity. Consequently $Z^0 \to b\bar{b}$ events were reweighted to reproduce the experimental uncertainty on the measured multiplicity [13]. The uncertainty on the number of background events rejected associated with this procedure was estimated to be 5 %.

Charm and bottom quark masses: The effect of changing the charm and bottom quark masses in the Monte Carlo, on the efficiency to select $g \to c\bar{c}$ and $g \to b\bar{b}$ events, was studied by generating Monte Carlo samples with a running charm quark mass in the range 1.1–1.4 GeV and bottom quark mass in the range 4.1–4.4 GeV. We estimated this effect to be 2% for the leptonic channels and 1.4% for the $D^{\star\pm}$ channel.

6.5 Other sources

Detector modelling: The resolution of the central tracking in the Monte Carlo had an effect on the predicted efficiencies and background. The simulated resolutions were varied by ±10 % relative to the values that optimally describe the data following the studies in [17]. The analysis was repeated and the efficiencies and background estimation were recalculated.

Monte Carlo Statistics: This was the uncertainty due to the finite size of the Monte Carlo samples used to determine the efficiencies and background.

7 Results and conclusions

The three measurements of the rate of secondary charm quark production are

$$g^{e}_{c\bar{c}} = 0.0303 \pm 0.0028 \pm 0.0041, \quad (7)$$

$$g^{\mu}_{c\bar{c}} = 0.0353 \pm 0.0037 \pm 0.0079, \quad (8)$$

$$g^{D^*}_{c\bar{c}} = 0.0408 \pm 0.0122 \pm 0.0069, \quad (9)$$

where the first uncertainty is statistical and the second systematic. By averaging the leptonic channels and taking into account correlations in the systematic uncertainties we obtain

$$g^{\ell}_{c\bar{c}} = 0.0311 \pm 0.0022 \pm 0.0042, \quad (10)$$

and combining this with the hadronic channel gives

$$g_{c\bar{c}} = 0.0320 \pm 0.0021 \pm 0.0038. \quad (11)$$

These results can be compared with the previous OPAL measurements [5,6]. As the values used for the rate of the process $g \to b\bar{b}$ and the branching ratio $B(c \to \ell)$ have changed since the previous publication, a comparison should be made after correcting for these effects. The old lepton results [6] should be scaled by a factor of 1.09. Thus the scaled results are $g^{e}_{c\bar{c}} = 0.0238 \pm 0.0033 \pm 0.0045$, $g^{\mu}_{c\bar{c}} = 0.0309 \pm 0.0063 \pm 0.0111$ and $g^{D^*}_{c\bar{c}} = 0.044 \pm 0.014 \pm 0.015$. The analyses described in this document use a larger data sample and different selection criteria than before. In particular, the different y_{cut} value and lepton momentum range resulted in a small overlap of the present data sample and the previous analysis sample. With these changes, less than one third of the current electron analysis data

Table 3. Summary of the systematic uncertainties on the measured $g_{c\bar{c}}$ values

Source of uncertainty	$\delta(g^{e}_{c\bar{c}})/g^{e}_{c\bar{c}}$ (%)	$\delta(g^{\mu}_{c\bar{c}})/g^{\mu}_{c\bar{c}}$ (%)	$\delta(g^{D^*}_{c\bar{c}})/g^{D^*}_{c\bar{c}}$ (%)
Lepton efficiency	4.9	5.8	-
Lepton mis-identification	2.5	18.4	-
Efficiency of photon conversion tagger	2.7	-	-
Dalitz decay multiplicities and efficiencies	1.4	-	-
Lepton transverse momentum	1.4	1.2	-
$D^{\star\pm}$ selection	-	-	7.1
$D^{\star\pm}$ background modelling	-	-	5.7
Λ_{QCD}	2.6	2.6	2.6
Parton shower mass cut-off	0.2	0.2	0.2
Primary hadron trans. mom. width (σ_q)	1.5	1.5	1.5
Lund symmetric fragmentation parameter b	1.8	1.8	1.8
JETSET - HERWIG - ARIADNE	4.1	4.1	4.5
$\langle x_E \rangle_b = 0.702 \pm 0.008$	1.1	1.0	2.7
$\langle x_E \rangle_c = 0.484 \pm 0.008$	1.3	1.3	3.5
Heavy quark fragmentation model	1.3	1.1	4.3
$b \to \ell$ model	0.1	0.1	-
$c \to \ell$ model	0.4	0.4	-
$b \to c \to \ell$ model	0.2	0.2	-
$B(b \to \ell)$=(10.99±0.23) %	0.4	0.4	-
$B(c \to \ell)$=(9.5±0.7) %	7.8	7.6	-
$B(b \to c \to \ell)$=(7.8±0.6) %	1.1	1.0	-
$B(b \to D^{\star\pm})$=(22.7±1.6) %	-	-	1.5
$B(c \to D^{\star\pm}) \times B(D^{\star\pm} \to D^0\pi)$=(15.3±1.5) %	-	-	7.0
$B(D^0 \to K\pi)$=(3.85±0.09) %	-	-	2.1
$\Gamma_{b\bar{b}}/\Gamma_{had}$=0.2170±0.0009	0.3	0.3	0.1
$\Gamma_{c\bar{c}}/\Gamma_{had}$=0.1734±0.0048	1.4	1.2	0.6
$g \to b\bar{b}$=(2.69±0.67)×10^{-3}	1.8	1.5	1.5
Jet mis-assignment	1.7	1.5	0.6
Jet mass cut	2.3	2.3	-
B hadron decay multiplicity	3.6	3.2	1.3
Charm and bottom quark masses	2.0	2.0	1.4
Detector resolution	2.5	1.9	6.1
Monte Carlo statistics	2.9	2.7	5.7
Total systematic uncertainty	**13.4**	**22.3**	**16.8**

sample overlaps the previous electron analysis. The increased momentum range of muons in this analysis resulted in having only 15 % of this muon sample common to the previous analysis. The previous $D^{\star\pm}$ analysis [5] used only 1.25 million hadronic Z^0 decays. Therefore, the number of common event to the present $D^{\star\pm}$ analysis is lower than 30 %. Taking into account these limited overlaps, the present and previous results differ by 1.7 standard deviations (taking into account statistical errors only). In addition, the present analysis is more comprehensive in the study of the systematic effects, hence, a large fraction of the systematic uncertainties are uncorrelated between the two analyses. Considering the uncorrelated part of the systematic uncertainties, the above difference is reduced below the level of one standard deviation and the two results can be considered as consistent.

In recent years, the OPAL data calibration has also been refined and the Monte Carlo simulation of the detector response had improved significantly. In view of these changes, the analysis presented in this paper is more accurate than the previous analysis in both the statistical significance and the proper description of the experimental environment. In conclusion, although the two results are statistically largely independent, they are dominated by systematic uncertainties, which are better understood for the new measurement. This result therefore supersedes the previous OPAL measurement.

The result presented in this paper, $g_{c\bar{c}}$=0.0320±0.0021 ±0.0038, is higher than all the theoretical predictions. In

particular, the most recent prediction ($g_{c\bar{c}}$=2.007 % [4]), which is higher than most other predictions, is 2.7 standard deviations below the result presented in this paper.

Acknowledgements. We particularly wish to thank the SL Division for the efficient operation of the LEP accelerator at all energies and for their continuing close cooperation with our experimental group. We thank our colleagues from CEA, DAPNIA/SPP, CE-Saclay for their efforts over the years on the time-of-flight and trigger systems which we continue to use. In addition to the support staff at our own institutions we are pleased to acknowledge the Department of Energy, USA, National Science Foundation, USA, Particle Physics and Astronomy Research Council, UK, Natural Sciences and Engineering Research Council, Canada, Israel Science Foundation, administered by the Israel Academy of Science and Humanities, Minerva Gesellschaft, Benoziyo Center for High Energy Physics, Japanese Ministry of Education, Science and Culture (the Monbusho) and a grant under the Monbusho International Science Research Program, Japanese Society for the Promotion of Science (JSPS), German Israeli Bi-national Science Foundation (GIF), Bundesministerium für Bildung, Wissenschaft, Forschung und Technologie, Germany, National Research Council of Canada, Research Corporation, USA, Hungarian Foundation for Scientific Research, OTKA T-029328, T023793 and OTKA F-023259.

References

1. M.H. Seymour, Nucl. Phys. B **436** (1995) 163
2. M.L. Mangano, P. Nason, Phys. Lett. B **285** (1992) 160
3. M.H. Seymour, Z. Phys. C **63** (1994) 99
4. D.J. Miller, M.H. Seymour, Phys. Lett. B **435** (1998) 213
5. OPAL Collab., R. Akers et al., Z. Phys. C **67** (1995) 27
6. OPAL Collab., R. Akers et al., Phys. Lett. B **353** (1995) 595
7. ALEPH Collab., R. Barate et al., Phys. Lett. B **434** (1998) 437
8. DELPHI Collab., P. Abreu et al., Phys. Lett. B **405** (1997) 202
9. OPAL Collab., K. Ahmet et al., Nucl. Instr. Meth. A **305** (1991) 275; OPAL Collab., P.P. Allport et al., Nucl. Instr. Meth. A **324** (1993) 34; OPAL Collab., P.P. Allport et al., Nucl. Instr. Meth. A **346** (1994) 476
10. OPAL Collab., G. Alexander et al., Z. Phys. C **52** (1991) 175
11. T. Sjöstrand, Comp. Phys. Comm. **82** (1994) 74; T. Sjöstrand, Comp. Phys. Comm. **39** (1986) 347; M. Bengtsson, T. Sjöstrand, Comp. Phys. Comm. **43** (1987) 367; T. Sjöstrand, Int. J. of Mod. Phys. A **3** (1988) 751
12. C. Peterson et al., Phys. Rev. D **27** (1983) 105
13. The LEP Collaborations, ALEPH, DELPHI, L3 and OPAL, Nucl. Instr. and Meth. A **378** (1996) 101; Updated averages are given in 'Input Parameters for the LEP Electroweak Heavy Flavour Results for Summer 1998 Conferences', LEPHF 98-01 (see http://www.cern.ch/LEPEWWG/heavy/); A Combination of Preliminary Electroweak Measurements and Constraints on the Standard Model, ALEPH, DELPHI, L3 and OPAL collaborations, the LEP Electroweak Working Group and the SLD Heavy Flavour and Electroweak Groups, CERN-EP/99-015
14. The Particle Data Group, C. Caso et al., Eur. Phys. J. C **3** (1998) 1
15. J. Allison et al., Nucl. Instr. Meth. A **317** (1992) 47
16. JADE Collab., W. Bartel et al., Z. Phys. C **33** (1986) 23; JADE Collab., S. Bethke et al., Phys. Lett. B **213** (1988) 235; S. Bethke et al., Nucl. Phys. B **370** (1992) 310; OPAL Collab., R. Akers et al., Z. Phys. C **63** (1994) 197
17. OPAL Collab., G. Abbiendi et al., Eur. Phys. J. C **8** (1999) 217
18. OPAL Collab., R. Akers et al., Z. Phys. C **60** (1993) 199
19. OPAL Collab., R. Akers et al., Z. Phys. C **66** (1995) 19
20. OPAL Collab., G. Abbiendi et al., Eur. Phys. J. C **8** (1999) 573
21. ARGUS Collab., H. Albrecht et al., Phys Lett B **374** (1996) 249
22. OPAL Collab., G. Alexander et al., Z. Phys C **69** (1996) 543
23. G. Marchesini, B.R. Webber et al., Comp. Phys. Comm. **67** (1992) 465
24. L. Lonnblad, Comp. Phys. Comm. **71** (1992) 15
25. P. Collins, T. Spiller, J. Phys. G **11** (1985) 1289
26. V.G. Kartvelishvili, A.K. Likehoded, V.A. Petrov, Phys. Lett. B **78** (1978) 615
27. OPAL Collab., G. Alexander et al., Phys. Lett. B **364** (1995) 93; OPAL Collab., G. Alexander et al., Z. Phys. C **72** (1996) 1
28. G.Altarelli et al., Nucl. Phys. B **208** (1982) 365
29. CLEO Collab., S. Henderson et al., Phys. Rev. D **45** (1992) 2212
30. DELCO Collab., W. Bacino et al., Phys. Rev. Lett. **43** (1979) 1073
31. MARK III Collab., R.M. Baltrusaitis et al., Phys. Rev. Lett. **54** (1985) 1976
32. CLEO Collab., D. Bortoletto et al., Phys. Rev. D **45** (1992) 21
33. N. Isgur, D. Scora, B. Grinstein, M. Wise, Phys. Rev. D **39** (1989) 799